

QUT Digital Repository:  
<http://eprints.qut.edu.au/>



Frost, Ray L. and Palmer, Sara J. and Spratt, Henry J. (2009) *Thermal decomposition of hydrotalcites with variable cationic ratios*.  
Journal of Thermal Analysis and Calorimetry, 95(1). pp. 123-129.

© Copyright 2009 Springer Science + Business Media

## Thermal decomposition of hydrotalcites with variable cationic ratios.

Sara J. Palmer, Henry J. Spratt, and Ray L. Frost\*

Inorganic Materials Research Program, School of Physical and Chemical Sciences, Queensland University of Technology, GPO Box 2434, Brisbane Queensland 4001, Australia.

### Abstract

Thermal analysis complimented with evolved gas mass spectrometry has been applied to hydrotalcites containing carbonate prepared by coprecipitation and with varying divalent-trivalent cation ratio. The resulting materials were characterized by XRD, and TGA/DTG to determine the stability of the hydrotalcites synthesised.

Hydrotalcites of formula  $Mg_4(Fe,Al)_2(OH)_{16}(CO_3,Cl).4H_2O$ ,  $Mg_6(Fe,Al)_2(OH)_{16}(CO_3,Cl).4H_2O$ , and  $Mg_8(Fe,Al)_2(OH)_{16}(CO_3,Cl).4H_2O$  formed by intercalation with the carbonate anion as a function of divalent/trivalent cationic ratio show variation in the d-spacing attributed to the size of the cation. The thermal decomposition of carbonate hydrotalcites consist of two decomposition steps between 300 and 400 °C, attributed to the simultaneous dehydroxylation and decarbonation of the hydrotalcite lattice. Water loss ascribed to dehydroxylation occurs in two decomposition steps, where the first step is due to the partial dehydroxylation of the lattice, while the second step is due to the loss of water interacting with the interlayer anions. Dehydroxylation results in the collapse of the hydrotalcite structure to that of its corresponding metal oxides, including  $MgO$ ,  $MgAl_2O_4$ , and  $MgFeAlO_4$ .

**Keywords:** hydrotalcite; pyroaurite; carbonate; X-ray Diffraction, thermal analysis

### Introduction

Hydrotalcites, or layered double hydroxides (LDH's) are fundamentally anionic clays, and are less well-known than cationic clays like smectites [1, 2]. The structure of hydrotalcite can be derived from a brucite structure ( $Mg(OH)_2$ ) in which e.g.  $Al^{3+}$  or  $Fe^{3+}$  (pyroaurite-sjögrenite) substitutes a part of the  $Mg^{2+}$  [3-14]. This substitution creates a positive layer charge on the hydroxide layers, which is compensated by interlayer anions or anionic complexes [15, 16]. When LDHs are synthesized any appropriate anion can be placed in the interlayer. These anions may be any anion with a suitable negative charge including the phosphate anion. The hydrotalcite may be considered as a gigantic cation which is counterbalanced by anions in the interlayer. In hydrotalcites a broad range of compositions are possible of the type  $[M^{2+}_{1-x}M^{3+}_x(OH)_2][A^{n-}]_{x/n}.yH_2O$ , where  $M^{2+}$  and  $M^{3+}$  are the di- and trivalent cations in the octahedral positions within the hydroxide layers with x normally between 0.17 and 0.33. It is normal practice to determine the composition of the formed hydrotalcite by chemical means such as ICP-AES or EDAX techniques.  $A^{n-}$  is an exchangeable interlayer anion [17]. In the hydrotalcites reevesite and pyroaurite, the divalent cations are  $Ni^{2+}$  and  $Mg^{2+}$  respectively with the trivalent cation being

---

\* Author to whom correspondence should be addressed (r.frost@qut.edu.au)

$\text{Fe}^{3+}$ . In these cases, the carbonate anion is the major interlayer counter anion. Normally the hydrotalcite structure based upon takovite (Ni,Al) and hydrotalcite (Mg,Al) has basal spacings of  $\sim 8.0 \text{ \AA}$  where the interlayer anion is carbonate. Reevesite and pyroaurite are based upon the incorporation of carbonate into the interlayer with  $d(001)$  spacings of around  $8 \text{ \AA}$  [18, 19].

Thermal analysis using thermogravimetric techniques enables the mass loss steps, the temperature of the mass loss steps and the mechanism for the mass loss to be determined [6, 11, 20-24]. Thermoanalytical methods provide a measure of the thermal stability of the hydrotalcite. The reason for the potential application of hydrotalcites as catalysts rests with the ability to make mixed metal oxides at the atomic level, rather than at a particle level. Such mixed metal oxides are formed through the thermal decomposition of the hydrotalcite [25, 26]. There are many other important uses of hydrotalcites such as in the removal of environmental hazards in acid mine drainage [27, 28], and a mechanism for the disposal of radioactive wastes [29]. Their ability to exchange anions presents a system for heavy metal removal from contaminated waters [30]. Structural information on different minerals has successfully been obtained recently by sophisticated thermal analysis techniques [6, 20-24]. In this work we report the infrared and near-infrared analysis of hydrotalcite with carbonate in the interlayer and explore the effect of divalent/trivalent ratio on hydrotalcite formation.

The decomposition of the Mg,Al hydrotalcite structure occurs in three steps:

- (i) removal of adsorbed water ( $< 100 \text{ }^\circ\text{C}$ ),
- (ii) elimination of the interlayer structural water ( $100 - 200 \text{ }^\circ\text{C}$ ), and
- (iii) the simultaneous dehydroxylation and decarbonation of the hydrotalcite framework ( $300 - 400 \text{ }^\circ\text{C}$ ) [6, 31-38].

A fourth decomposition step may occur for the loss of either a volatile anion species (e.g.  $\text{Cl}^-$ ,  $\text{NO}_3^-$ , and  $\text{CO}_3^{2-}$ ) or a non-volatile species in which the anion is included in the formation of a mixed metal oxide [31, 35, 38]. The determination of the decomposition steps of hydrotalcite depends on the dryness of the sample, stability of the interlamellar species, and possible guest-host interactions mobilising the hydroxyl groups in the hydrotalcite lattice [35]. The thermal decomposition of carbonate hydrotalcites consist of two decomposition steps between  $300$  and  $400 \text{ }^\circ\text{C}$ , attributed to the simultaneous dehydroxylation and decarbonation of the hydrotalcite lattice. Water loss ascribed to dehydroxylation occurs in two decomposition steps, where the first step is due to the partial dehydroxylation of the lattice, while the second step is due to the loss of water interacting with the interlayer anions. Dehydroxylation results in the collapse of the hydrotalcite structure to that of its corresponding metal oxides, including  $\text{MgO}$ ,  $\text{Al}_2\text{O}_3$ , and  $\text{MgAl}_2\text{O}_4$  (at temperatures over  $900^\circ\text{C}$ ) [6, 33]. The exact decomposition product relies on the hydrotalcite and its counter balancing anions.

Thermal analysis has proven most useful for the study of the thermal stability of hydrotalcites [11, 39-42]. The objective of this research is to determine the thermal stability of hydrotalcites synthesised with different divalent/trivalent cationic ratio.

## Experimental

### *Preparation of Mixed Metal Ion Solution*

Varying amounts of aluminium chloride hexahydrate, iron(III) chloride hexahydrate and magnesium chloride hexahydrate were dissolved in 500mL of water. The ratio of moles of  $M_{2+}$  to  $M_{3+}$ , where M is a metal, in the different solutions were: 2:1, 3:1 and 4:1. The following table summarises how much of each metal was dissolved in 500mL of water.

	<i>2:1 Solution</i>	<i>3:1 Solution</i>	<i>4:1 Solution</i>
<i>Magnesium</i>	67.765g	76.24g	81.32g
<i>Aluminium</i>	11.11g	8.335g	6.665g
<i>Iron(III)</i>	22.525g	16.895g	13.515g

The chosen metal ion solution was then added drop wise into the caustic solution via a peristaltic pump. The solution was then vacuum filtered, washed well with hot degassed water and dried in an oven overnight at 120°C.

### *X-ray diffraction*

X-Ray diffraction patterns were collected using a Philips X'pert wide angle X-Ray diffractometer, operating in step scan mode, with Cu  $K_{\alpha}$  radiation (1.54052 Å). Patterns were collected in the range 3 to 90° 2 $\theta$  with a step size of 0.02° and a rate of 30s per step. Samples were prepared as a finely pressed powder into aluminium sample holders. The Profile Fitting option of the software uses a model that employs twelve intrinsic parameters to describe the profile, the instrumental aberration and wavelength dependent contributions to the profile.

### *Thermal Analysis*

Thermal decomposition of the hydrotalcite was carried out in a TA® Instruments incorporated high-resolution thermogravimetric analyzer (series Q500) in a flowing nitrogen atmosphere (80 cm<sup>3</sup>/min). Approximately 50 mg of sample was heated in an open platinum crucible at a rate of 5.0 °C/min up to 1000°C at high resolution. With the quasi-isothermal, quasi-isobaric heating program of the instrument the furnace temperature was regulated precisely to provide a uniform rate of decomposition in the main decomposition stage. The TGA instrument was coupled to a Balzers (Pfeiffer) mass spectrometer for gas analysis. Only selected gases such as water and carbon dioxide were analyzed.

## Results and discussion

### *X-ray diffraction*

The X-ray diffraction patterns for the carbonate interlayer hydrotalcites are shown in Figure 1a. Hydrotalcite normally has a  $d_{(003)}$  spacing of around 7.9 Å. The sulphate interlayer hydrotalcite has a spacing of 8.0 Å. The XRD patterns show that the d-spacing for the carbonate interlayer hydrotalcite is cation dependent.

The XRD patterns obtained for the synthetic hydrotalcites match closely with reference pattern 01-070-2150 (pyroaurite –  $(\text{Fe}_2\text{Mg}_6(\text{OH})_{16}\text{CO}_3(\text{H}_2\text{O})_{4.5})_{0.375}$ ). The method of synthesis for these hydrotalcites allows for the possibility of a variety of products including: hydrotalcite, pyroaurite, and other forms of hydrotalcites with a mixture of cationic ratios. However, there appears to be only one phase present in the XRD pattern, suggesting that multiple phases were not produced. Minor quantities may have been produced but were not detected using XRD. The  $d_{(003)}$  obtained for the synthesised hydrotalcites were 7.72, 7.97, and 7.91 Å, 2:1, 3:1, and 4:1 hydrotalcite respectively. The increase in  $d$  spacing for the 3:1 and 4:1 hydrotalcites indicates an increase in the interlayer region of these hydrotalcites. The reason for this is attributed to the increased degree of surface hydroxyls resulting in an increased degree of filling in the hydrotalcite interlayer.

### ***Thermogravimetry***

The dehydroxylation step for hydrotalcite is generally observed at around 300°C [6, 31-38]. The results obtained in this investigation agree with literature, with dehydroxylation occurring at 322, 324, and 312°C for the 2:1, 3:1, and 4:1 hydrotalcites respectively. The point of dehydroxylation can be used as an indication of the thermal stability of the hydrotalcite, where a delay in dehydroxylation (higher temperature) indicates increased thermal stability. In regards to the hydrotalcites synthesised it is observed that the 3:1 hydrotalcites is more stable than the 2:1 and 4:1 hydrotalcites, with the 4:1 hydrotalcite having the lowest stability. This decrease in stability in the 4:1 hydrotalcite is caused by the increased positive charge of the brucite-like layers, which would require a larger number of anions to counter-balance the charge. The dTG curve for the 2:1 hydrotalcite distinctly shows 2 mass loss steps, corresponding to first dehydroxylation and then decarbonation. However, for the 3:1 and 4:1 hydrotalcites only a single mass loss step is observed indicating that dehydroxylation and decarbonation occur simultaneously. The ion current curves for all hydrotalcite show water vapour and  $\text{CO}_2$  evolve at these temperatures. The mass spectrometer detected chloride gases ( $m/Z = 35$  and  $32$ ) in all three of the hydrotalcites synthesised, figures not shown. This suggests that chloride was intercalated into the hydrotalcites along with carbonate, however carbonate was the more dominant anion.

### ***2:1 Metal ion solution***

The thermogravimetric and differential thermogravimetric analysis of 2:1 hydrotalcites of proposed formula  $\text{Mg}_4(\text{Fe,Al})_2(\text{OH})_{16}(\text{CO}_3,\text{Cl})\cdot 4\text{H}_2\text{O}$  is shown in Figure 2a. The ion current curves for selected evolved gases are shown in Figure 2b. A very small mass loss step between 25 and 42°C of 0.76% is observed and attributed to the loss of physisorbed water. Over the temperature range 42 and 200°C, a mass loss of 14.42% is observed and attributed to the loss of water in the interlayer of the hydrotalcite structure. The  $m/Z=17$  and  $18$  ion current curves display a broad peak over this temperature range, indicating the removal of the remained of the adsorbed water on the hydrotalcite surface. The following thermal decomposition is proposed:  $\text{Mg}_4(\text{Al,Fe})_2(\text{OH})_{16}(\text{CO}_3,\text{Cl})\cdot x\text{H}_2\text{O} \rightarrow \text{Mg}_6\text{Al}_2(\text{OH})_{16}(\text{CO}_3,\text{Cl}) + x\text{H}_2\text{O}$ . Two mass loss steps are observed at 322 and 338°C with a total mass loss of 24.48%. The ion current curves for  $m/Z=17$  and  $18$  show two maxima at around 325 and 340°C attributed to evolved water vapour at these temperatures confirming the loss of OH

units at these temperatures. The ion current curves for  $m/Z=44$  and  $12$  show maxima at  $\sim 350^\circ\text{C}$  confirming the evolution of  $\text{CO}_2$  at this temperature attributed to the thermal decomposition of the carbonate anion. The following reaction is proposed:  $\text{Mg}_4(\text{Al,Fe})_2(\text{OH})_{16}(\text{CO}_3,\text{Cl}) \rightarrow \text{MgAl}_2\text{O}_4 + 5\text{MgO} + \text{MgFeAlO}_4 + \text{CO}_2 + 8\text{H}_2\text{O}$ . The decomposition products proposed were confirmed by XRD analysis (Figure 1b). The molecular mass of this compound is between 531 and 614 molecular mass units, dependent on which cation is substituted into the brucite-like layer ( $\text{Al}^{3+}$  or  $\text{Fe}^{3+}$ ) and the anions in the interlayer. The theoretical mass loss according to this reaction of water vapour and  $\text{CO}_2$  is 27.16% and 8.30%. A higher temperature mass loss at around  $830^\circ\text{C}$  of 2.82% is observed and is assigned to the loss of oxygen from the decomposition of the oxides.

### *3:1 Metal ion solution*

The thermogravimetric analysis of 3:1 hydrotalcites of proposed formula  $\text{Mg}_6(\text{Fe,Al})_2(\text{OH})_{16}(\text{CO}_3,\text{Cl}) \cdot 4\text{H}_2\text{O}$  is shown in Figure 3a. The ion current curves for selected evolved gases are shown in Figure 3b. The molecular mass of this compound is between 580 and 662 molecular mass units, dependent on which cation is substituted into the brucite-like layer ( $\text{Al}^{3+}$  or  $\text{Fe}^{3+}$ ) and the anions in the interlayer. The mass loss over the temperature range 25 to  $65^\circ\text{C}$  is 0.58% attributed to the loss of adsorbed water. The ion current curves for  $m/Z=17$  and  $18$  prove water is the evolved gas at this temperature range. A further mass loss of 12.75% at  $145^\circ\text{C}$  is observed. Again the ion current curves indicate that water vapour is evolved at these temperatures. These mass losses are attributed to the loss of water from the interlayer of the hydrotalcite. A broad mass loss step is observed at  $324^\circ\text{C}$  with a total mass loss of 26.68%. The ion current curves for  $m/Z=17$  and  $18$  show a broad maxima at around  $311^\circ\text{C}$  with a shoulder present at  $354^\circ\text{C}$  attributed to evolved water vapour at these temperatures confirming the loss of OH units at these temperatures. The ion current curves for  $m/Z=44$  and  $12$  show two maxima at  $314$  and  $\sim 350^\circ\text{C}$  confirming the evolution of  $\text{CO}_2$  at this temperature. The evolution of gases attributed to both OH and carbonate units suggests the simultaneous dehydroxylation and decarbonation of the hydrotalcite structure occurs at this temperature. The following reaction is proposed:  $\text{Mg}_4(\text{Al,Fe})_2(\text{OH})_{16}(\text{CO}_3,\text{Cl}) \rightarrow \text{MgAl}_2\text{O}_4 + \text{MgFeAlO}_4 + 5\text{MgO} + \text{CO}_2 + 8\text{H}_2\text{O}$ . The decomposition products proposed were confirmed by XRD analysis (Figure 1c). The theoretical mass losses according to this formula of  $\text{CO}_2$  and OH units are 5.17 and 24.82%, respectively.

### *4:1 Metal ion solution*

The thermogravimetric and differential thermogravimetric curves for the thermal decomposition of the 4:1 hydrotalcite is shown in Figure 4a. The proposed formula for the 4:1 hydrotalcite is  $\text{Mg}_6(\text{Fe,Al})_2(\text{OH})_{16}(\text{CO}_3,\text{Cl}) \cdot 4\text{H}_2\text{O}$ . The ion current curves for selected evolved gases are shown in Figure 4b. Thus the molecular mass is between 653 and 686 AMU, dependent on the cationic composition of the hydrotalcite and the anion(s) intercalated into the hydrotalcite structure. The theoretical mass loss due to dehydroxylation is 20.31%.

A mass loss step of 7.16% at low temperatures is observed at around  $65^\circ\text{C}$ , attributed to the removal of water adsorbed on the surface. A further mass loss step of 7.91% at  $135^\circ\text{C}$  is attributed to the dehydration of the hydrotalcite interlayer. The ion

current curves prove the evolution of water vapour at the corresponding temperatures. A single mass loss of 26.31% is found at 312°C. The ion current curves of  $m/Z=17$  and 18 prove that water is the evolved gas at this temperature. This water vapour results from the dehydroxylation of the hydrotalcite. The evolution of gases attributed to both OH and carbonate units suggests the simultaneous dehydroxylation and decarbonation of the hydrotalcite structure occurs at this temperature. The following reaction is proposed:  $Mg_8(Al,Fe)_2(OH)_{16}(CO_3,Cl) \rightarrow MgAl_2O_4 + MgFeAlO_4 + 5MgO + CO_2 + 8H_2O$ . The decomposition products proposed were confirmed by XRD analysis (Figure 1d).

The experimental mass loss of 21.42% may be compared with the theoretical mass loss of 20.31%.

## Conclusions

The decomposition of the synthesised hydrotalcites occurred in 3 steps, (1), evaporation of adsorbed water (up to 100 °C), (2), elimination of the interlayer structural water (up to 200 °C), and (3), dehydroxylation and decarbonation of the hydrotalcite framework (up to 400 °C). The ion current curve revealed that dehydroxylation and decarbonation occurred simultaneously. Dehydroxylation indicates the thermal stability of the hydrotalcite structure, where delays in dehydroxylation indicate a more stable hydrotalcite. Therefore, the order of stability for the synthesised hydrotalcites is 3:1, 2:1 and 4:1 cationic ratios. The collapse of the hydrotalcite structure produced corresponding metal oxides, including MgO,  $MgAl_2O_4$ , and  $MgFeAlO_4$ .

## Acknowledgements

The financial and infra-structure support of the Queensland Research and Development Centre (QRDC-Alcan) and the Queensland University of Technology Inorganic Materials Research Program of the School of Physical and Chemical Sciences is gratefully acknowledged. One of the authors (SJP) is grateful to Alcan for a Masters scholarship. The Australian Research Council (ARC) is thanked for funding the Thermal Analysis Facility.

## References

- [1] K. Hashi, S. Kikkawa, M. Koizumi, *Clays and Clay Minerals* 31 (1983) 152-154.
- [2] L. Ingram, H.F.W. Taylor, *Mineralogical Magazine and Journal of the Mineralogical Society (1876-1968)* 36 (1967) 465-479.
- [3] J.T. Kloprogge, L. Hickey, R.L. Frost, *Mater. Chem. Phys.* 89 (2005) 99-109.
- [4] L. Frost Ray, L. Erickson Kristy, *Spectrochimica acta. Part A, Molecular and biomolecular spectroscopy* 61 (2005) 51-56.
- [5] K.L. Erickson, T.E. Bostrom, R.L. Frost, *Mater. Lett.* 59 (2004) 226-229.
- [6] R.L. Frost, K.L. Erickson, *J. Therm. Anal. Calorim.* 76 (2004) 217-225.
- [7] R.L. Frost, K.L. Erickson, *Thermochim. Acta* 421 (2004) 51-58.
- [8] J.T. Kloprogge, L. Hickey, R.L. Frost, *J. Raman Spectrosc.* 35 (2004) 967-974.
- [9] J.T. Kloprogge, L. Hickey, R.L. Frost, *J. Solid State Chem.* 177 (2004) 4047-4057.
- [10] R.L. Frost, Z. Ding, *Thermochim. Acta* 405 (2003) 207-218.
- [11] R.L. Frost, W. Martens, Z. Ding, J.T. Kloprogge, *J. Therm. Anal. Calorim.* 71 (2003) 429-438.
- [12] R.L. Frost, M.L. Weier, M.E. Clissold, P.A. Williams, *Spectrochim. Acta, Part A* 59 (2003) 3313-3319.
- [13] R.L. Frost, M.L. Weier, M.E. Clissold, P.A. Williams, J.T. Kloprogge, *Thermochim. Acta* 407 (2003) 1-9.
- [14] R.L. Frost, M.L. Weier, J.T. Kloprogge, *J. Raman Spectrosc.* 34 (2003) 760-768.
- [15] R.M. Taylor, *Clay Minerals* 17 (1982) 369-372.
- [16] H.F.W. Taylor, *Mineralogical Magazine and Journal of the Mineralogical Society (1876-1968)* 37 (1969) 338-342.
- [17] H.C.B. Hansen, C.B. Koch, *Applied Clay Science* 10 (1995) 5-19.
- [18] D.L. Bish, A. Livingstone, *Mineralogical Magazine* 44 (1981) 339-343.
- [19] E.H. Nickel, R.M. Clarke, *American Mineralogist* 61 (1976) 366-372.
- [20] E. Horvath, J. Kristof, R.L. Frost, N. Heider, V. Vagvolgyi, *J. Therm. Anal. Calorim.* 78 (2004) 687-695.
- [21] R.L. Frost, M.L. Weier, K.L. Erickson, *J. Therm. Anal. Calorim.* 76 (2004) 1025-1033.
- [22] R.L. Frost, K.L. Erickson, *J. Therm. Anal. Calorim.* 78 (2004) 367-373.
- [23] E. Horvath, J. Kristof, R.L. Frost, A. Redey, V. Vagvolgyi, T. Cseh, *J. Therm. Anal. Calorim.* 71 (2003) 707-714.
- [24] J. Kristof, R.L. Frost, J.T. Kloprogge, E. Horvath, E. Mako, *J. Therm. Anal. Calorim.* 69 (2002) 77-83.
- [25] F. Rey, V. Fornes, J.M. Rojo, *J. Chem. Soc., Faraday Trans.* 88 (1992) 2233-2238.
- [26] M. Valcheva-Traykova, N. Davidova, A. Weiss, *J. Mater. Sci.* 28 (1993) 2157-2162.
- [27] G. Lichti, J. Mulcahy, *Chemistry in Australia* 65 (1998) 10-13.
- [28] Y. Seida, Y. Nakano, *Journal of Chemical Engineering of Japan* 34 (2001) 906-911.
- [29] Y. Roh, S.Y. Lee, M.P. Elless, J.E. Foss, *Clays and Clay Minerals* 48 (2000) 266-271.
- [30] Y. Seida, Y. Nakano, Y. Nakamura, *Water Research* 35 (2001) 2341-2346.

- [31] E.L. Crepaldi, P.C. Pavan, J.B. Valim, *Journal of the Brazilian Chemical Society* 11 (2000) 64-70.
- [32] J.I. Di Cosimo, V.K. Diez, M. Xu, E. Iglesia, C.R. Apesteguia, *Journal of Catalysis* 178 (1998) 499-510.
- [33] R.L. Frost, A.W. Musumeci, T. Bostrom, M.O. Adebajo, M.L. Weier, W. Martens, *Thermochimica Acta* 429 (2005) 179-187.
- [34] T. Lopez, E. Ramos, P. Bosch, M. Asomoza, R. Gomez, *Materials Letters* 30 (1997) 279-282.
- [35] F. Malherbe, J.-P. Besse, *Journal of Solid State Chemistry* 155 (2000) 332-341.
- [36] S. Miyata, *Clays and Clay Minerals* 28 (1980) 50-56.
- [37] J. Perez-Ramirez, G. Mul, J.A. Moulijn, *Vibrational Spectroscopy* 27 (2001) 75-88.
- [38] D. Tichit, M.H. Lhouty, A. Guida, B.H. Chiche, F. Figueras, A. Auroux, D. Bartalini, E. Garrone, *Journal of Catalysis* 151 (1995) 50-59.
- [39] J. Bouzaid, R.L. Frost, *J. Therm. Anal. Calorim.* 89 (2007) 133-135.
- [40] J.M. Bouzaid, R.L. Frost, W.N. Martens, *J. Therm. Anal. Calorim.* 89 (2007) 511-519.
- [41] R.L. Frost, A.W. Musumeci, M.O. Adebajo, W. Martens, *J. Therm. Anal. Calorim.* 89 (2007) 95-99.
- [42] R.L. Frost, J.M. Bouzaid, A.W. Musumeci, J.T. Klopogge, W.N. Martens, *J. Therm. Anal. Calorim.* 86 (2006) 437-441.

**List of Figures:**

Figure 1a: XRD patterns and references for the synthesised hydrotalcites with varying cationic ratios.

Figure 1b: XRD patterns of the synthesised 2:1 hydrotalcite after thermal analysis treatment.

Figure 1c: XRD patterns of the synthesised 3:1 hydrotalcite after thermal analysis treatment.

Figure 1c: XRD patterns of the synthesised 3:1 hydrotalcite after thermal analysis treatment.

Figure 2a: TGA/dTG of the synthesised 2:1 hydrotalcite.

Figure 2a: TGA/dTG of the synthesised 2:1 hydrotalcite.

Figure 3a: TGA/dTG of the synthesised 3:1 hydrotalcite.

Figure 3a: TGA/dTG of the synthesised 3:1 hydrotalcite.

Figure 4a: TGA/dTG of the synthesised 4:1 hydrotalcite.

Figure 4a: TGA/dTG of the synthesised 4:1 hydrotalcite.

Figures:

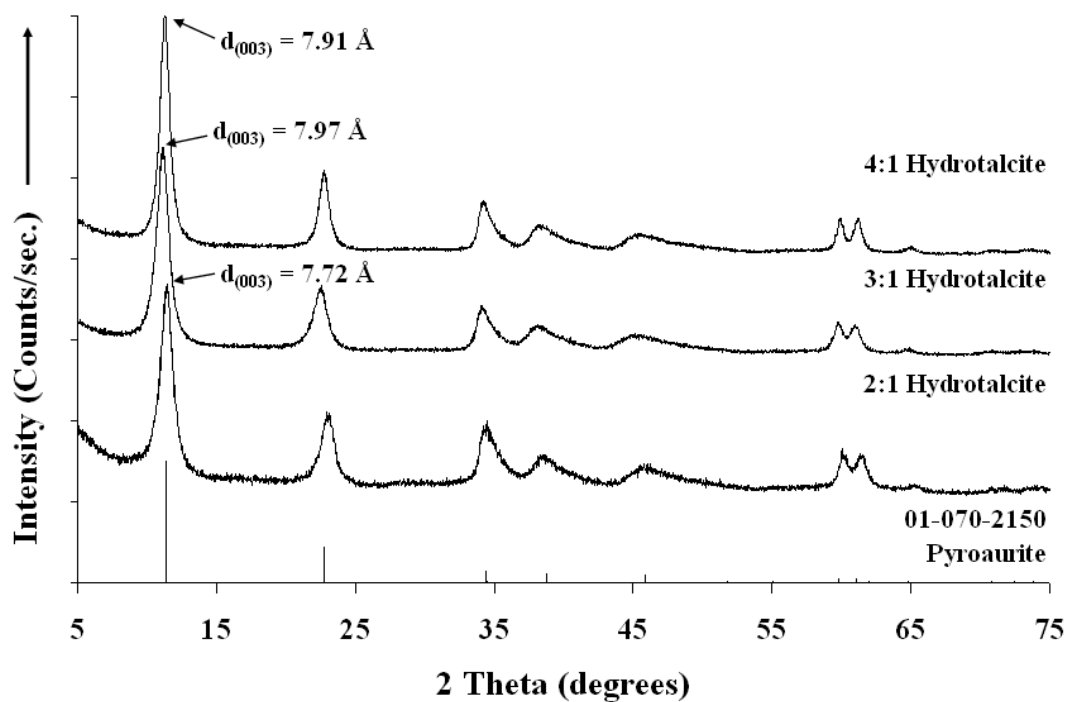


Figure 1a: XRD patterns and references for the synthesised hydrotalcites with varying cationic ratios.

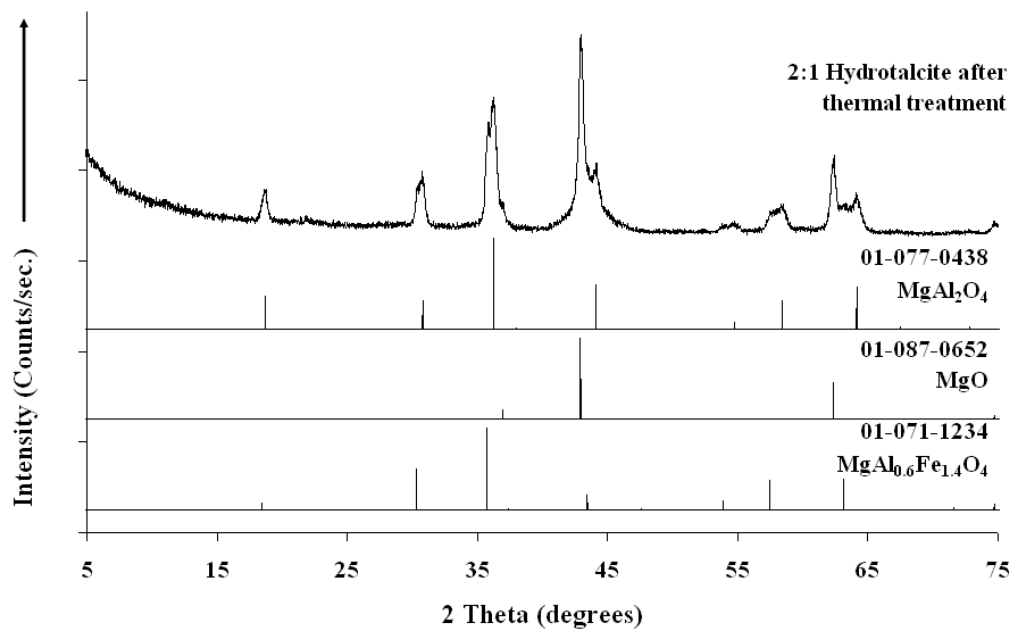


Figure 1b: XRD patterns of the synthesised 2:1 hydrotalcite after thermal analysis treatment.

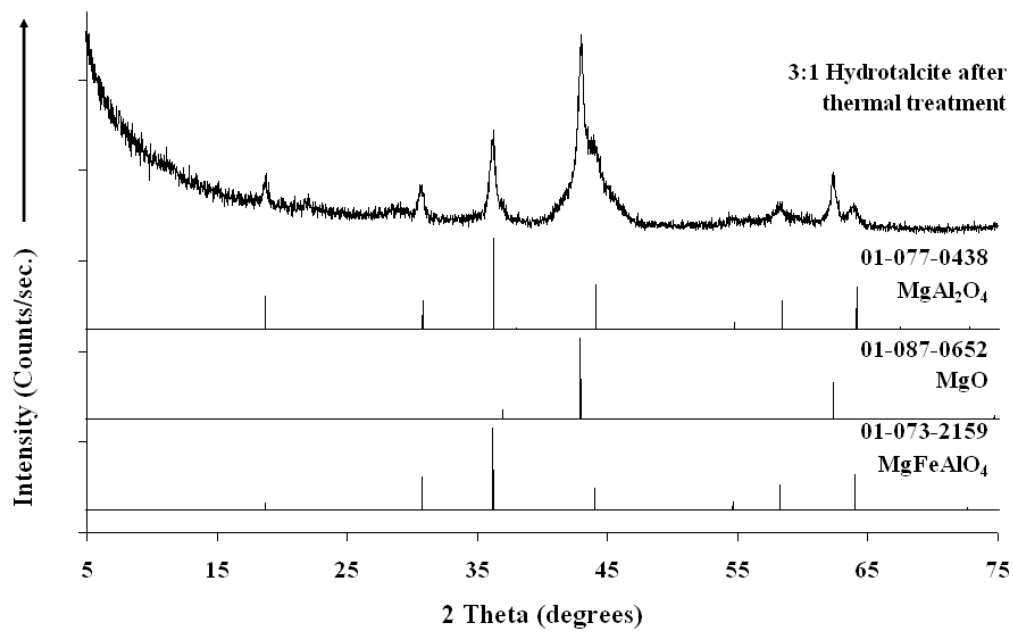


Figure 1c: XRD patterns of the synthesised 3:1 hydrotalcite after thermal analysis treatment.

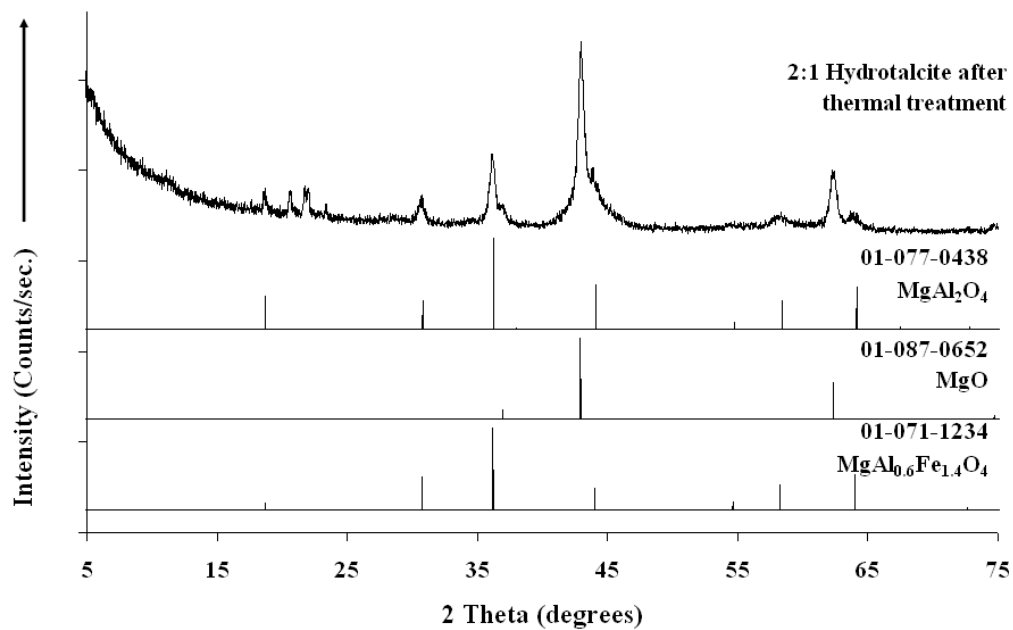


Figure 1d: XRD patterns of the synthesised 4:1 hydrotalcite after thermal analysis treatment.

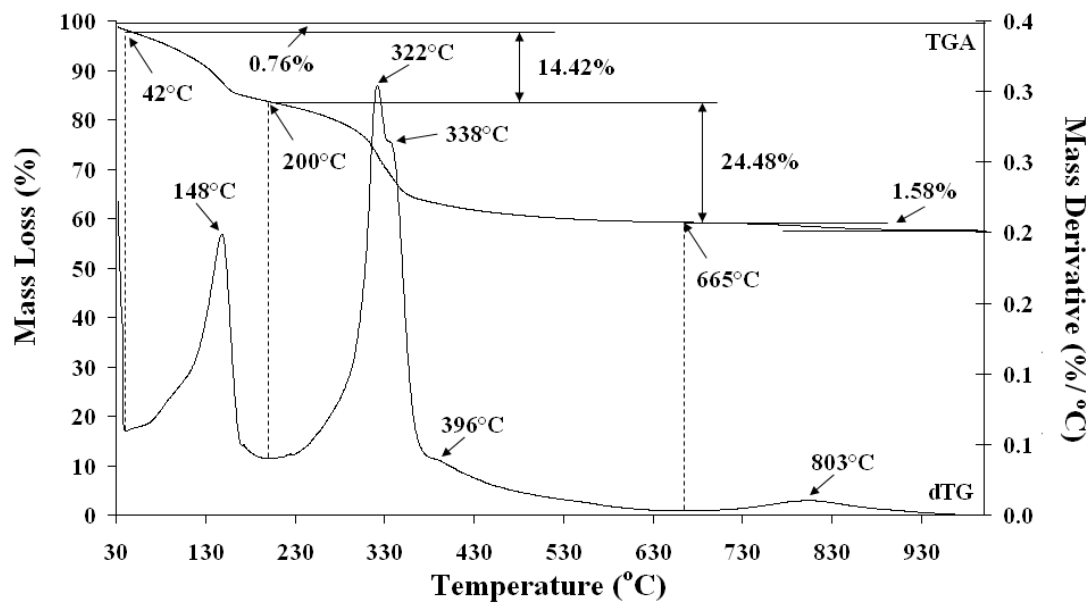


Figure 2a: TGA/dTG of the synthesised 2:1 hydrotalcite.

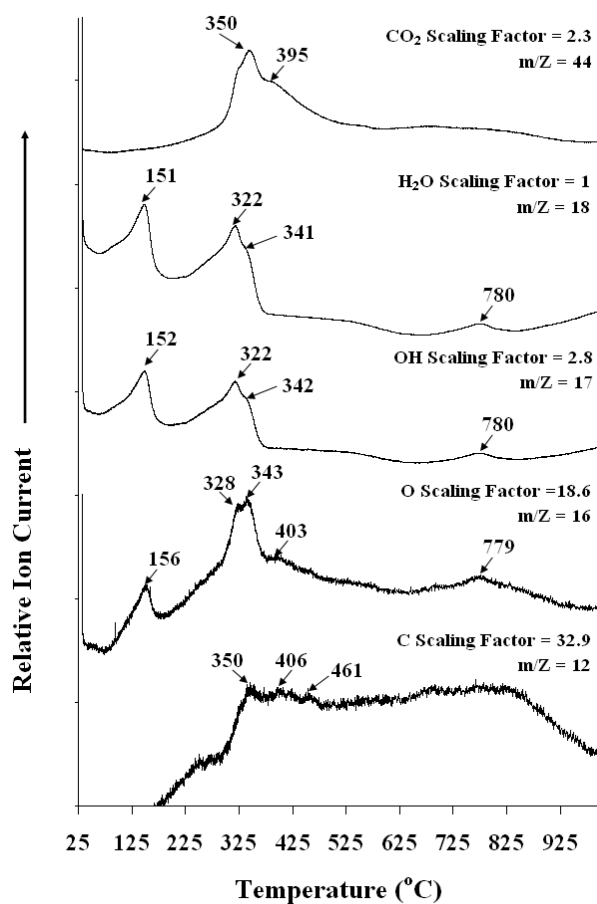


Figure 2b: Mass spectroscopy data of the synthesised 2:1 hydrotalcite.

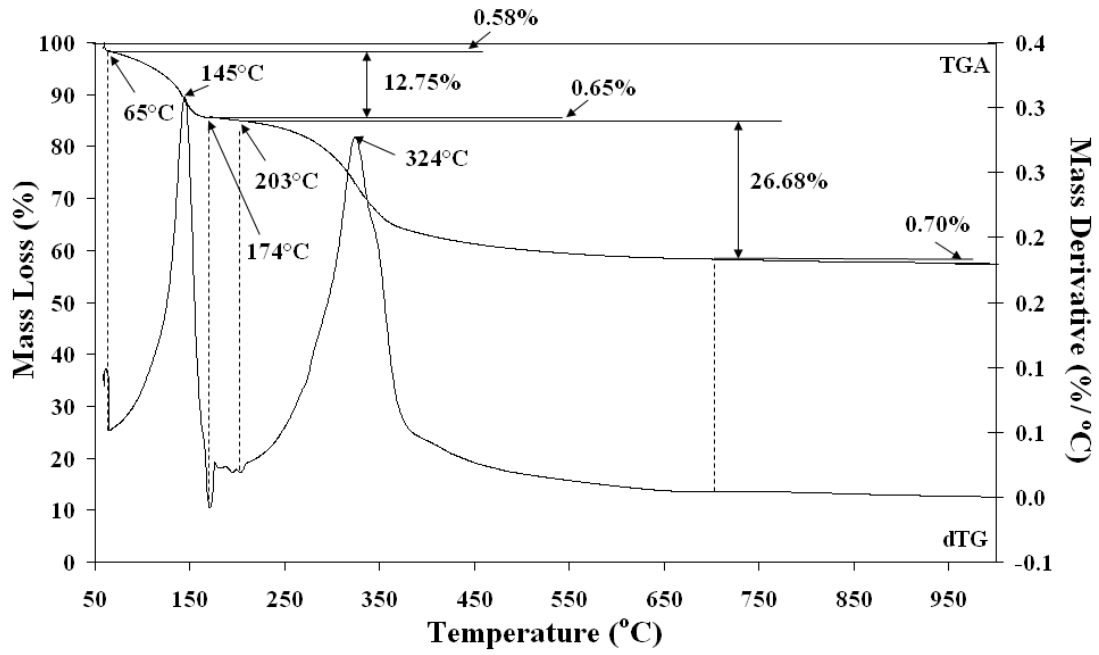


Figure 3a: TGA/dTG of the synthesised 3:1 hydrotalcite.

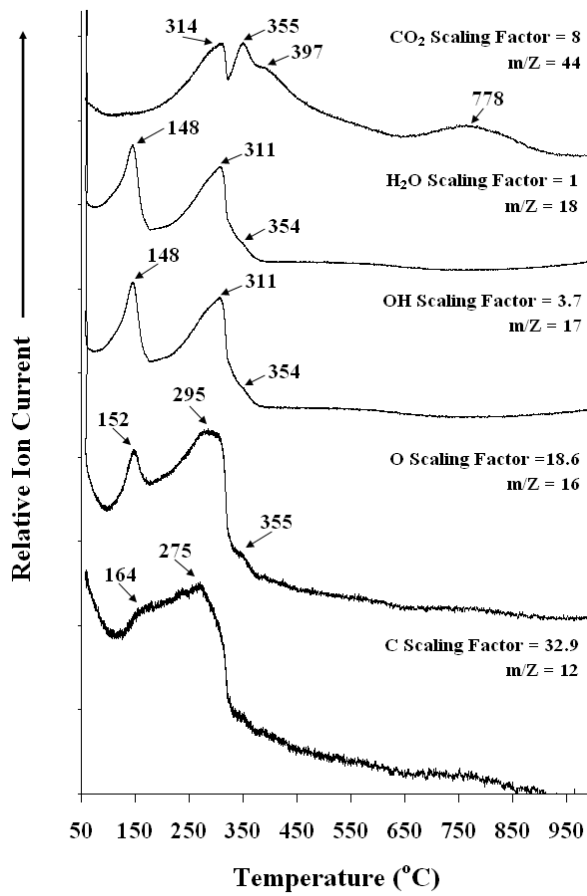


Figure 3b: Mass spectroscopy data of the synthesised 3:1 hydrotalcite.

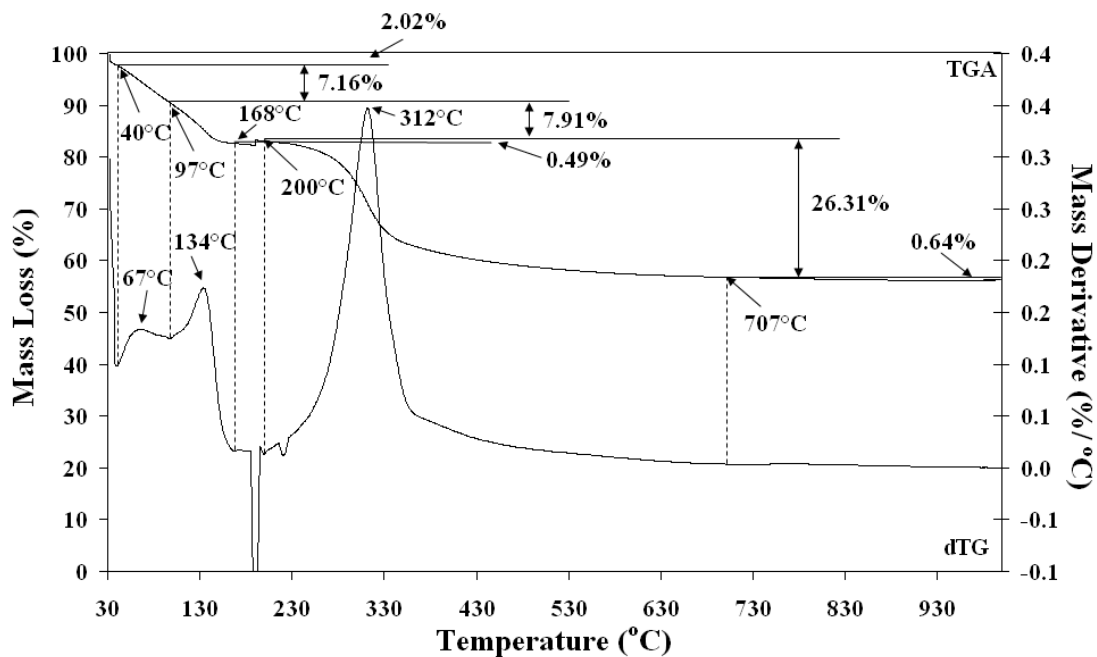


Figure 4a: TGA/dTG of the synthesised 4:1 hydrotalcite.

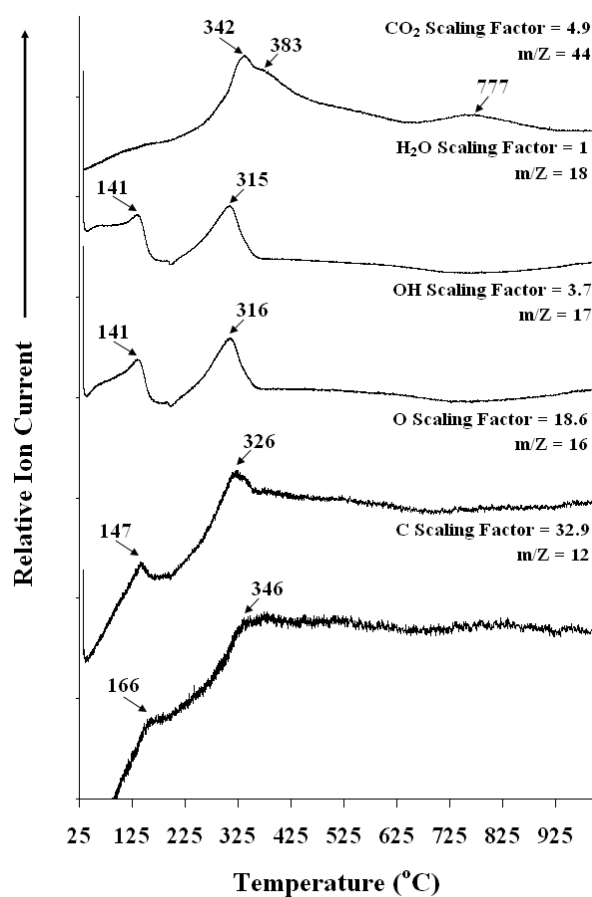


Figure 4b: Mass spectroscopy data of the synthesised 4:1 hydrotalcite.